Examining the frictional forces between mixed hydrophobic – hydrophilic alkylsilane monolayers

José L. Rivera, G. Kane Jennings, and Clare McCabe

Citation: J. Chem. Phys. **136**, 244701 (2012); doi: 10.1063/1.4729312
View online: http://dx.doi.org/10.1063/1.4729312
View Table of Contents: http://jcp.aip.org/resource/1/JCPSA6/v136/i24
Published by the AIP Publishing LLC.

Examining the frictional forces between mixed hydrophobic – hydrophilic alkylsilane monolayers

José L. Rivera,[1,2,3,a)] G. Kane Jennings,[1] and Clare McCabe[1,4,a)]
[1]*Department of Chemical and Biomolecular Engineering, Vanderbilt University, Nashville, Tennessee 37235, USA*
[2]*Facultad de Ingeniería Química, Universidad Michoacana de San Nicolás de Hidalgo, Morelia, 58000 Michoacán, México*
[3]*Instituto de Investigaciones en Materiales, Universidad Nacional Autónoma de México, Apartado Postal 70-360, 04510 México DF, México*
[4]*Department of Chemistry, Vanderbilt University, Nashville, Tennessee 37235, USA*

(Received 9 February 2012; accepted 29 May 2012; published online 25 June 2012)

Monolayers presenting methyl-terminated (hydrophobic) and hydroxyl-terminated (hydrophilic) surfaces on silica have been studied by molecular dynamics simulation and the effects of hydrogen bonding, chain length, and chain mixing on the frictional properties determined. The hydroxyl-terminated monolayers were found to show large adhesion zones as a result of strong interfacial interlayer hydrogen bonds; the interfacial sliding forces observed in the hydroxyl-terminated monolayers being one order of magnitude higher than the interfacial forces for the hydrophobic surfaces at the characteristic point of zero-load. Mixed hydroxyl- and methyl-terminated monolayers of equal length were found to exhibit intermediate shear stress values between those observed for pure monolayers, with the magnitude of the shear stress depending on the surface content of the hydroxyl-terminated chains. For mixed monolayers of unequal chain lengths, at high loads a maximum in the magnitude of the shear stress as a function of the length of the methyl-terminated chain was observed due to the creation of a buffer zone between the hydroxyl-terminated chains that produces strong hydrogen-bonding interactions. The effect of a constant normal load or constant separation simulation ensemble on the results has also been studied and in general found to have minimal influence on the observed behavior, although some differences are observed for the shear stress at intermediate normal loads due to the formation of stronger hydrogen bond networks at constant load compared to constant separation. © *2012 American Institute of Physics*. [http://dx.doi.org/10.1063/1.4729312]

I. INTRODUCTION

Understanding and controlling the forces acting in microelectromechanical (MEMS) and nanoelectromechanical (NEMS) devices, where surfaces are in normal and/or sliding contact, is of critical importance to the wide-spread commercial realization and successful operation of such systems.[1] These devices are typically fabricated from silicon; however, silicon oxidizes easily, forming an exterior layer that contains hydrogen-bonding groups.[2–4] Due to the nature of these surface hydroxyl groups, silica has a high friction coefficient and high wear rate. Effective lubrication is therefore central to the successful operation of durable devices with moving parts and the control of adhesion, friction, and wear. Traditional lubricants (oils) have been shown to be too viscous to infiltrate the channels and crevices of MEMS/NEMS devices and provide only modest protection.[5,6] As a result, alternative lubrication schemes have been investigated, such as thin-film coatings of diamond-like carbon and self-assembled monolayers (SAMs).[7–9]

A wide range of SAMs on different surfaces have been studied by both experiment and simulation (see, for example, the reviews of Harrison *et al.*,[10] Zhang and Mylvaganam,[11] and Bhushan[9]). Monolayer films prepared from *n*-alkyltrichlorosilanes on silicon[12–15] and *n*-alkanethiols on gold[15] have been shown to greatly decrease sliding friction coefficients by reducing the interaction strength between the sliding probe and the surface. A particular advantage of these monolayers is the ability to tailor the surface/probe interactions by using different terminal groups on the adsorbate and different monolayer thickness by varying the chain length of the adsorbate.[15] For example, it has been shown experimentally that friction decreases in alkylsilane films as the length of the alkane portion of the monolayer chain increases up to C_{12},[16] because the longer chains pack more effectively, creating a smoother interface, which in turn reduces friction. For longer chains ($>C_{12}$), the friction forces tend to an asymptotic value.[17–21]

In this work, the frictional properties of sliding OH-terminated monolayers have been investigated using molecular simulations over a wide range of normal loads for the first time. Although such surfaces have high friction forces due to their high surface energy, the presence of water between hydrophilic terminated monolayers has been shown to reduce frictional properties considerably, even at very low water concentrations when the water molecules do not condense.[22,23] Furthermore, surfaces coated with OH-terminated chains

a)Authors to whom correspondence should be addressed. Electronic addresses: c.mccabe@vanderbilt.edu and rivera_jose_l@yahoo.com.

have the possibility to serve as a support for lubricants that can weakly attach to these surfaces through hydrogen bonding and so allows the creation of new lubricating systems, where not only the contact surface is important for the tribological behavior, but also the friction forces between the OH-terminated surface and the lubricant. Through tuning of the chain length of one of the components in a mixed monolayer system, a bound-mobile lubrication scheme can also be studied. Bound-mobile lubrication couples the stability of a bound layer with the mobility of a liquid or liquid-like layer in order to provide both good frictional properties as well as good durability.[24–30]

The frictional behavior of contacting surfaces containing functional groups that can form hydrogen bonds is complex and depends on a number of factors, including the length and flexibility of the chains that attach the hydrogen bond forming groups to the surface,[31,32] the surface coverage and separation of the chains,[19,23,33,34] temperature,[35] *p*H,[36] surface disorder,[19] sliding velocity,[20] etc. The frictional properties of self-assembled monolayers of alkanethiol molecules on gold surfaces containing COOH-terminal groups have been studied experimentally and compared to the properties of alkanethiol molecules containing CH_3- terminal groups; at zero-load hydrogen bonds formed in the COOH- terminated monolayers results in friction forces ~17 times higher than those for monolayers with CH_3-terminal groups.[37,38] Similar results have been found in simulations of self-assembled monolayers of OH-terminated alkanethiols on gold tips,[39] with the friction forces shown to be mostly due to the breaking and formation of intra- and interlayer hydrogen bonds; while the number of intralayer hydrogen bonds remained almost constant as a function of load, the number of interlayer hydrogen bonds increased rapidly over the range of normal loads studied.[40] Simulations of self-assembled monolayers of OH-terminated alkanethiols on gold tips have also shown that surfaces covered with these alkanethiols are less easily penetrated by a tip than CH_3-terminated alkanethiol monolayers and therefore show improved antiwear properties.[31]

Here, we study the frictional behavior of alkylsilanes with OH-terminated chains and examine the effect of normal load from weak interacting distances to normal loads near the rupture of silica. Results for CH_3-terminated chains are also reported for comparison purposes. The influence of the length of the alkylsilane chain on the friction forces and the effect of mixing OH-terminated chains with CH_3-terminated chains at different surface concentrations has also been studied. Finally, the use of longer CH_3-terminated chains mixed with the OH-terminated chains to create a bound-mobile lubrication scheme has been examined.

II. SIMULATION DETAILS

The simulated systems are composed of two opposing silica surfaces coated with functionalized alkylsilanes. The structure of the silica surfaces corresponds to the ideal β-cristoballite,[41,42] which is composed of tetrahedral SiO_4 alternatively pointing up and down in a layered hexagonal lattice. Six tetrahedral SiO_4 layers were used yielding a thickness of ~12 Å and an area of 53.87×46.66 Å^2. In constructing the silicon surfaces, there are two possible surfaces of silica onto which the alkylsilane chains can be chemisorbed; when the outer layer of the silica surface consists of tetrahedra pointing outwards, each tetrahedra has three oxygen sites to chemisorb the alkylsilane chains (high surface density) and when the tetrahedra are pointing inwards, each tetrahedra has only one site to chemisorb the alkylsilane chains (low surface density). In this work, an alkylsilane chain was chemisorbed onto one of the three oxygen atoms of the high surface density layer, as this produces a surface density of ~25 Å^2 per chain and is similar to reported experimental values for full coverage.[43,44] Using this approach 100 chains were attached to each silica surface, which has been shown in previous simulation studies to be large enough to avoid any system size effects.[18]

The force field parameters for the silica surface are based on the optimized potentials for liquid simulations (OPLS) all-atom potential[45] and have been used previously to simulate the frictional behavior of methyl-terminated,[46,47] and fluorinated[48] coatings chemisorbed on silica. The methyl- and hydroxyl-terminated chains were modeled using the OPLS all-atom potentials for alkanes and alcohols, respectively.[45] The simulations were carried out using the LAMMPS molecular dynamics code.[49] Electrostatic interactions were computed using the particle-particle particle-mesh algorithm in 2D.[50] Electrostatic and Lennard-Jones interactions were computed using a cutoff radius of 10 Å. Long-range corrections were not used. All interactions were computed under periodic boundary conditions in the surface plane to simulate an infinite surface. All systems were simulated at 300 K using the Nose-Hoover thermostat,[51–53] and the equations of motion integrated using the multiple time step algorithm rRESPA,[54] with time steps of 0.125 fs for bonded interactions, 0.250 fs for angle interactions (both valence and dihedral), and 0.50 fs for all intermolecular interactions.

Simulations were performed in both the constant separation (CS) and constant normal load (CL) ensembles to determine the effect, if any, of the simulation conditions on the results. In the CS ensemble, the separation between the outermost layer of silicon atoms in the top and bottom monolayers is fixed and a constant velocity of 5 m/s is imposed in each sliding direction, with the two monolayers moving in opposite directions and so yields a net sliding velocity of 10 m/s. Previous studies at shear velocities in the range from cm/s to m/s have shown a weak dependency between the friction forces and the shear velocity, while the trends in the shear stress behavior did not change in the range of shear velocities studied.[20] This is also consistent with the work of Chandross *et al.*[18] and Lorenz *et al.*[48] who observed no frictional dependence on sliding velocity for either fluorocarbon or hydrocarbon monolayer systems at moderate loads. The movement of the outermost layer of atoms in the normal direction is restricted by setting the normal and lateral forces to zero during the simulations. The CL ensemble also restricts movement in the lateral direction in the same way as the CS ensemble, but applies external forces to produce a constant normal load rather than a constant separation. In the CL ensemble, the normal load and shear stresses are calculated as the sum of the intermolecular interactions between the monolayers before setting the forces in the normal and

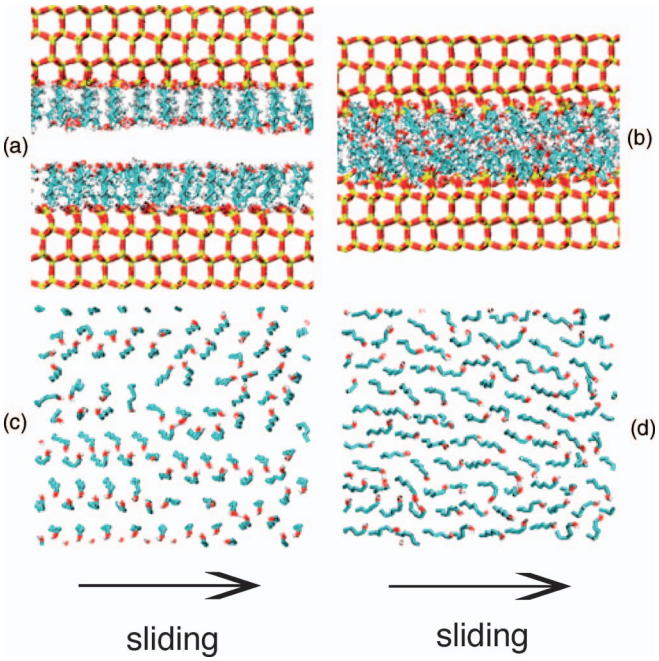

FIG. 1. Snapshots of $-Si(OH)_2(CH_2)_6OH$ monolayers at (a) near zero-load and zero-adhesion state (separation 49 Å) and (b) at ~3.25 GPa (separation 38 Å), under sliding at a constant velocity of 10 m/s and 300 K. Top-down views at near zero-load and zero-adhesion (c) and at ~3.25 GPa (d) are also shown. Light blue spheres represent carbon atoms, red oxygens, gray hydrogens, and yellow silicons. In (c) and (d) the hydrogen atoms of the CH_2 groups are not shown for clarity.

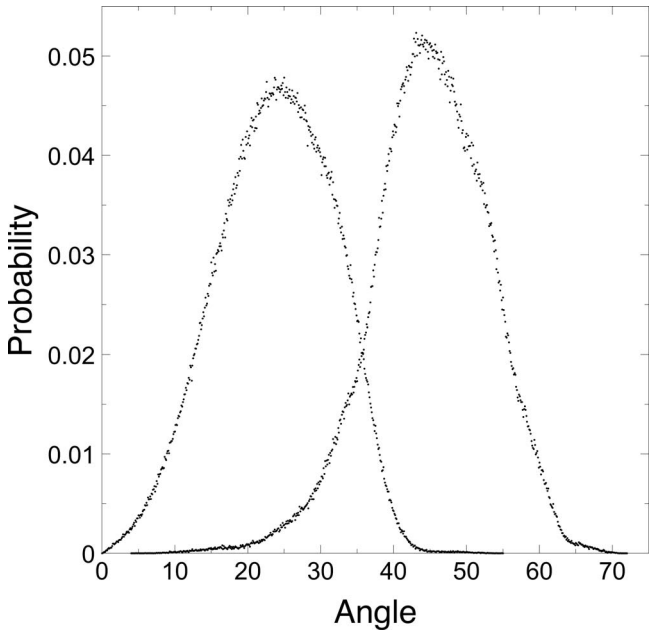

FIG. 2. Distribution of tilt angles observed in $-Si(OH)_2(CH_2)_6OH$ monolayers at near zero-load state (left curve) and at ~3.25 GPa (right curve) under sliding at a constant velocity of 10 m/s and 300 K.

sliding directions, respectively, to zero. Previous simulations of interacting chains with simple interactions (van der Waals forces), using CS and CL ensembles have been shown to produce different results,[55] and which ensemble produces a better approximation for specific experimental setups has been debated.[56,57] In this work, we explore the effects of the ensemble on systems that involve hydrogen-bonding interactions, which has not been previously examined.

III. RESULTS

A. Pure OH-terminated monolayers

The structural and frictional properties of pure $-Si(OH)_2(CH_2)_6(OH)$ monolayers in contact under shear in both the CS and CL ensembles was first studied and their frictional properties compared to those of pure alkyl-terminated monolayers of similar chain length [i.e., $-Si(OH)_2(CH_2)_5(CH_3)$]. Although the number of carbon atoms is the same in both systems, the length of the OH terminated chains is slightly longer than the CH_3-terminated chains due to the size of the hydroxyl group relative to hydrogen. Snapshots of sliding states of the OH-terminated monolayers at very low (~0 GPa) and very high (~3.25 GPa) normal loads are shown in Figs. 1(a) and 1(b), respectively. After an equilibration period of 0.25 ns, the chains reorganize in order to minimize unfavorable steric interactions, as shown in the top down views of Figs. 1(c) and 1(d), from which we can see that at high normal loads the CH_2 groups are exposed, reflecting the tilting of the chains. The tilt angle of the chains can be defined by the angle between the vector normal to the silica surface and the line between the silicon atom of the alkylsilane and the oxygen atom of the terminal OH group of the chain. As expected, in the simulations the average tilt angle of the OH-terminated chains increases (by ~20° from 23.75° to 44.5°) when the load changes from 0 to ~3.25 GPa in both ensembles (CS and CL), as seen in the probability distributions of Fig. 2. In previous work, we reported similar tilt angles for CH_3-terminated surfaces sliding at 10 m/s and also observed that the tilt angle increases at higher sliding velocities.[46] Experimentally, the average tilt angles obtained for *n*-octadecylsiloxane chains (C_{18})[58,59] are found to be small (10°–13°) for surface coverages between 86%–98%; however, we note that in the experimental systems crosslinking between the chains occurs and the films will likely contain defects, unlike those studied in a simulation. If we compare the results obtained from the simulations at the near zero-load and zero-adhesion state, which corresponds to a state in which the monolayers still interact, but the repulsive and attractive interactions in the normal direction are balanced and on average are zero and so the monolayers are expected to be unaffected by the presence of the opposite layer (even under sliding), we find that our results (including the previously reported CH_3-terminated layers)[46] are ~10° higher than experimental values. The higher tilt angles observed in the simulations are presumably due to a combination of the stability generated by the periodically replicated defect-free silica surface in the simulations and possible force field effects, since the force fields used were originally parameterized for the study of bulk fluids.

At very low loads, chains within the layer interact through intralayer hydrogen bonds forming rows of hydrogen bonds parallel to the sliding direction. At very high loads, the

TABLE I. Number of hydrogen bonds for $-Si(OH)_2(CH_2)_6OH$ monolayers under sliding at a constant velocity of 10 m/s and 300 K. A hydrogen bond is defined by oxygen – hydrogen and oxygen – oxygen separations of less than 2.6 Å and 3.6 Å, respectively, following the work of Kelkar *et al.*[60]

			Interlayer		Intralayer	
Ensemble	Load (GPa)	Separation(Å)	Total	Matching	Total	Matching
CS	∼0.15	42	147	90	22	8
	∼3.25	38	73	40	52	11
CL	0		154	68	18	5
	3		118	56	25	4

tilt angles of the chains reach an average value of 45° and an ordered hydrogen bond network is no longer observed; however, due to the short separation between the monolayers, intermolecular hydrogen bonds between the two monolayers are observed, with hydrogen bonds continuously forming and breaking as the sliding progresses. To provide insight into this behavior, the average number of hydrogen bonds was determined from the simulations as a function of separation and is reported in Table I. If the two chain ends belong to the same monolayers an intralayer hydrogen bond is formed, otherwise an interlayer is formed. Looking at Table I and the results from the CS simulations, we can see that on average at high loads (∼3.25 GPa) approximately half of the interlayer hydrogen bonds formed at low loads (∼0.15 GPa) are observed. This is perhaps to be expected, as although the terminal OH-groups are present at the contact surface, the high load increases the number of repulsive interactions leaving the terminal groups with less opportunity to interact through attractive interactions (hydrogen bonds). Interestingly, the number of intralayer hydrogen bonds increases by more than 50% when the load is increased from ∼0.15 to 3.25 GPa. This is presumably a related effect, in that, if the terminal OH-groups have less opportunity to interact with the terminal OH-groups in the opposite layer due to the increasing number of repulsive interactions, they will be forced to interact more closely with the OH-groups within the same monolayer. In Fig. 3, the distribution of intermolecular hydrogen bonds as a function of the hydrogen-oxygen distance at separations of 42 Å, which corresponds to a normal load of 0 GPa and 38 Å (normal load ∼3.25 GPa) are presented. From the figure, we can see that the distribution of hydrogen bonds for the separation of 42 Å has a peak at ∼1.89 Å and a minimum at ∼2.6 Å. The position of the peak is similar to the normal hydrogen bond distance of bulk water at the same temperature,[61] indicating that the end OH-groups intermolecularly associate as in bulk water, even though their coordination and dynamics are influenced by the sliding process. Furthermore, the results obtained for the peak and minimum in the hydrogen-bonding histograms for the sliding hydroxyl chains are in agreement with those reported from simulations of alcohols in the bulk.[60] For the interlayer separation of 38 Å (normal load ∼3.25 GPa), the number of hydrogen bonds decreases considerably over the value seen at 42 Å (∼0.15 GPa), as can be seen by the reduced distribution of intermolecular oxygen-hydrogen atoms with separations less than 2.6 Å in Fig. 3. The trend in the number of interlayer hydrogen bonds observed in Table I

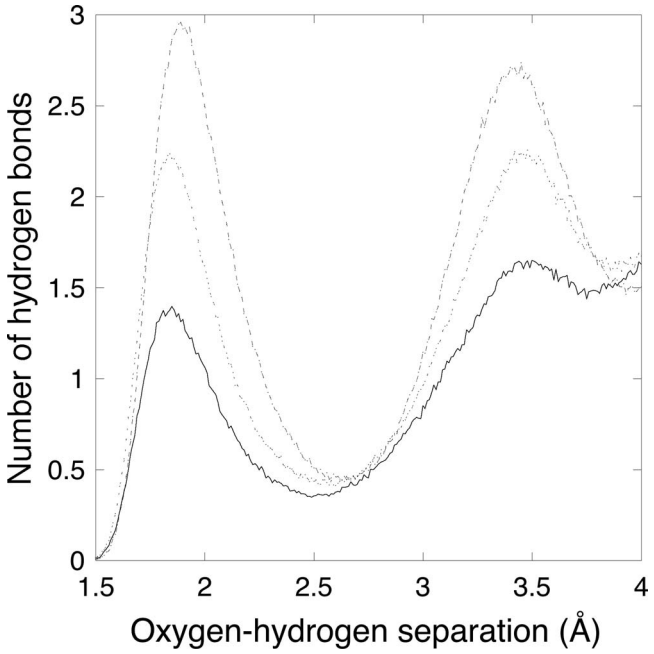

FIG. 3. Distribution of hydrogen bonds for $-Si(OH)_2(CH_2)_6OH$ monolayers as a function of the oxygen-hydrogen separation at constant separations of 38 Å (solid line), and 42 Å (slashed line), and constant load of 3 GPa (dotted line).

when the normal load changes from 0.15 to 3.25 GPa, is also observed in the peaks of Fig. 3; the peak at 3.25 GPa is around half the magnitude of the peak at 0.15 GPa. The higher normal load also affects the position of the first minimum, which for a normal load of 3.25 GPa decreases to ∼2.5 Å.

In order to obtain a more complete view of the interactions between the layers, the number of hydrogen bonds formed between the corresponding rows of chains in the top and bottom surfaces was also measured. We define a *matching* hydrogen bond as one formed between the hydroxyl groups in two corresponding rows and a hydrogen bond as non-matching when it is formed between hydroxyl groups in offset rows. The calculated average number of matching hydrogen bonds is also reported in Table I. At low loads (∼0.15 GPa) around 3/5 of the average total hydrogen bonds are between corresponding rows. If we consider that rows are separated by ∼4.7 Å, we can conclude that the sliding process results in a continuous lateral tilting of the chains and a cycle of corresponding hydrogen bonds forming and then breaking, the chains bending laterally, and then hydrogen bonds forming and breaking between non-corresponding chains. When the load is increased to ∼3.25 GPa the number of matching hydrogen bonds decreases by 50%, as was observed for the total number of hydrogen bonds.

Previous simulations of CH_3-terminated chains on silica have reported that the normal load under sliding and the separation between the monolayers are directly proportional;[40,46] however, for OH-terminated chains we find that the behavior is more complex due to the strong adhesive forces between the monolayers as a result of hydrogen bonds between the OH groups in the two opposing monolayers. The dependence of the separation of the monolayers (measured as the distance between the outermost layers of silicon atoms in each silica

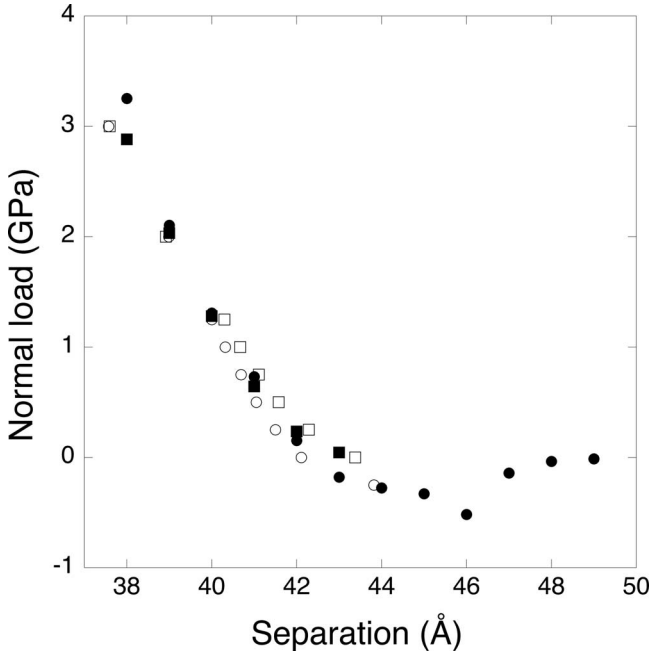

FIG. 4. Normal load as a function of separation for $–Si(OH)_2(CH_2)_6OH$ (circles) and $Si(OH)_2(CH_2)_5CH_3$ (squares) monolayers simulated under constant separation (filled symbols) and constant normal load (open symbols) at a sliding velocity of 10 m/s and 300 K. Standard deviations of the data are smaller than the size of the symbols, except for the system with OH-terminated chains, using the constant load ensemble, which shows standard deviations of up to 0.25 Å at the average separation of 43.82 Å.

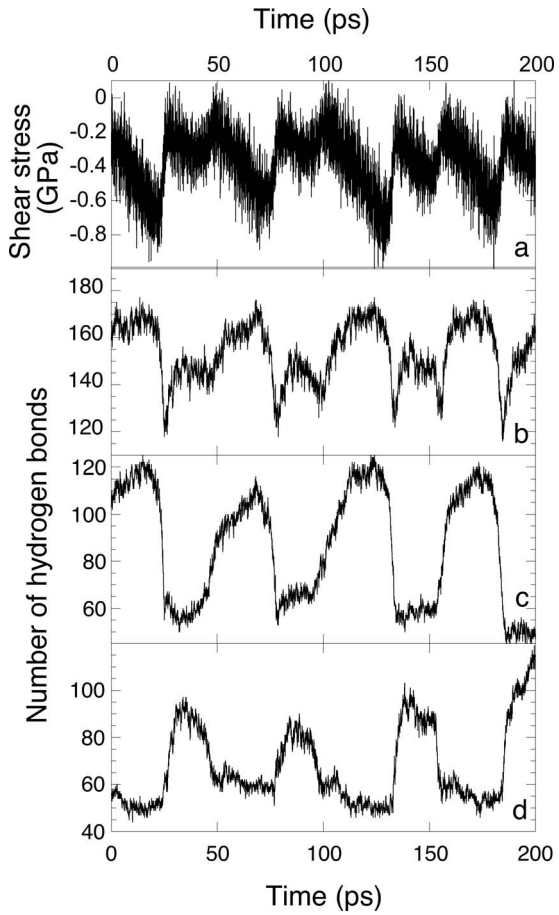

FIG. 5. Shear stress (a) and number of (b) interlayer hydrogen bonds, (c) interlayer non-matching hydrogen bonds, and (d) interlayer matching hydrogen bonds, as a function of time for $–Si(OH)_2(CH_2)_6OH$ monolayers simulated at 300 K and a constant separation of 42 Å and sliding velocity of 10 m/s.

surface) on the normal load under sliding is shown in Fig. 4 for CH_3- and OH-terminated chains in both the CS and CL ensembles. From Fig. 4, we can see that the normal load curve for OH-terminated monolayers using the CS ensemble crosses the *x* axis twice and represents force balances between adhesive and external forces; the adhesion zone, characterized by negative loads, extends for ∼6.7 Å. The first intercept (∼42 Å) represents the transition from repulsive to adhesive states, while the second (∼49 Å) represents the transition from adhesive to non-adhesive states, characterized by a zero-load and zero-adhesion, and is the point at which no load nor adhesion forces exist between the monolayers. The chains in the monolayers at both zero-load intercepts are well ordered and extended, with the total number of hydrogen bonds observed essentially the same; however, the number of intralayer hydrogen bonds is higher at the second intercept, as interlayer hydrogen bonds are not observed at a separation of 49 Å. We note that the adhesion zone shows a minimum at the separation of 46 Å and that the distance between the position of the minimum and the position where the normal load changes from negative to positive values is ∼3.4 Å, which is slightly larger than the oxygen – oxygen van der Waals radius employed in the simulations (3.12 Å). Once the normal load takes positive values, chains in the OH- and CH_3-terminated monolayers behave similarly, presumably because the van der Waals forces in the normal direction are dominating the interactions between the monolayers at positive loads.

By analyzing the shear stress profiles and the formation/breaking of hydrogen bonds as a function of the simulation time, we can study the dynamics of the chains during the sliding process, the results of which are reported for the separation of 42 Å in Fig. 5. The shear stress shows clear periodic behavior indicating stick-slip behavior with a period of ∼50 ps, which corresponds to the time needed for one chain to pass over another chain at 10 m/s in the sliding direction. The stick of the chains takes most of the time period and has a complex behavior; for approximately half of the 50 ps, the shear stress remains almost constant (∼ −0.3 GPa), while for the other half the shear stress increases gradually to the maximum value (∼ −0.8 GPa), after which the slip of the chains occurs within a few ps. Within the stick and slip period, the formation and breakage of hydrogen bonds also exhibits two separate phenomena. In the first part (∼25–50 ps), when the shear stress remains almost constant, the number of matching interlayer hydrogen bonds doubles in magnitude before they break at the end of the 25 ps period. In the second half of the process (∼50 ps–75 ps), as the shear stress increases slowly, the number of non-matching hydrogen bonds doubles in magnitude; they then break, slip occurs, and the shear stress suddenly decreases. We can therefore conclude that the slip process primarily involves the breaking of non-matching hydrogen bonds. This is also supported by the animation provided in the supplementary material.[62]

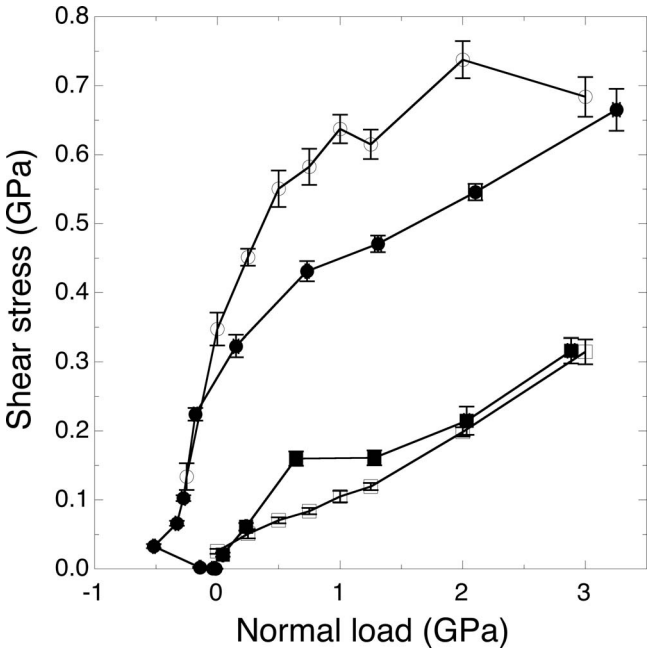

FIG. 6. Shear stress as a function of normal load at a sliding velocity of 10 m/s and 300 K for silica coated with $-Si(OH)_2(CH_2)_6OH$ chains at constant separation (filled circles) and constant normal load (open circles). Results for the $-Si(OH)_2(CH_2)_5CH_3$ monolayers are also shown for constant separation (filled squares) and constant load (open squares) ensembles. Lines are provided as a guide to the eye.

Compared to the CS simulations, we find that the simulations performed in the CL ensemble produce essentially the same separations at loads up to 2 GPa for both OH-terminated and CH_3-terminated chains, as shown in Fig. 4. Above 2 GPa, differences between the CL and CS ensembles are observed for the OH-terminated chains. The differences between the two ensembles above 2 GPa can be attributed to the fact that under a CL ensemble the molecules are able to reorganize more easily than in the CS ensemble through fluctuations in the separation distance;[63] the reorganization allows more closely packed structures to be formed, which reduces the volume between the monolayers and, therefore, reduces the separation between the layers. When comparing the results from the two different ensembles, the effect on the friction forces for OH-terminated chains was found to be stronger than the effect observed on the normal load. To illustrate, in Fig. 6 the shear stress as a function of load for OH-terminated and CH_3-terminated chains simulated in both ensembles is reported. Shear stresses in the OH-terminated monolayers are 0.273 GPa (CS) and 0.347 GPa (CL), which are between 13 and 17 times, respectively, higher than that for CH_3-terminated monolayers at zero-load (0.021 GPa, CL). In the adhesion zone (negative loads) for the OH-terminated monolayers, the friction forces show positive values intersecting the zero-load line at 0.27 (CS) and 0.34 GPa (CL) in the shear stress, while for the CH_3-terminated monolayers both curves intersect the zero-load line at ~0.02 GPa. AFM simulations and experiments have both shown a similar ratio between the friction forces of CH_3-terminated and OH-terminated chains at zero-loads and found that friction forces of OH-terminated chains are an order of magnitude higher than CH_3-terminated chains.[37–39] Additionally, experiments using interfacial force microscopy to study the friction forces as a function of the normal force for self-assembled COOH-terminated alkanethiol chains on gold with similar chain length as studied in this work show the same behavior as that reported herein; a large zone of negative normal forces with positive friction forces and non-zero friction forces intersecting the normal zero-force axis.[37] The only simulated system that shows a linear behavior over the complete range of loads studied is the CH_3-terminated chains under the CL ensemble; a linear regression produces a friction coefficient of ~0.1 and is similar to that obtained in previous simulation work.[19]

For the OH-terminated chains, the CL ensemble produces higher shear stresses than the CS ensemble at positive loads, with both systems reporting essentially the same value at very high (>3 GPa) normal loads. For the CH_3-terminated chains, the CL ensemble produces the opposite effect, with the shear stresses being lower than those seen in the CS ensemble. We note that similar behavior has been reported in sliding studies of hydrogen-terminated silicon.[63] As for the OH-terminated chains, at very low and very high loads the friction forces for the CH_3-terminated chains are very similar in both ensembles. As described in Sec. II, in the simulated systems the surface coverage is 100% (i.e., a chain is bonded to each surface silicon site), which leads to a chain separation of ~5 Å and is considerably larger than the C–C van der Waals radius, resulting in the terminal atoms of each chain having some freedom to move in the surface plane. The CL ensemble enhances the chain freedom for short periods of time and allows the molecules to reorganize and minimize unfavorable steric interactions more easily than in the CS ensemble, producing lower shear stresses for systems dominated by short-range dispersion interactions in the sliding direction (i.e., CH_3-terminated chains), and higher shear stresses for systems dominated by long-range Coulombic forces in the sliding direction (OH-terminated chains). The animation of the CL simulation provided in the supplementary material[62] illustrates how the chains in the OH-terminated monolayers organize in the CL ensemble; hydrogen bonds form in the surface plane, followed by an expansion in the system volume in the normal direction as the two surfaces move relative to each other, the hydrogen bonds then break and the system returns to its original separation.

Hydrogen bond formation was also monitored in the CL simulations and the average total number of hydrogen bonds calculated and reported in Fig. 3 and Table I in order to compare to the results at constant separation. Comparing the distribution of hydrogen bonds as a function of the oxygen – hydrogen separation obtained in the CL ensemble at 3 GPa with those from the CS ensemble at a separation of 38 Å (average load of ~3.25 GPa), we find the peak in the distribution of hydrogen bonds is located at essentially the same hydrogen-oxygen separation in both ensembles, though the CL simulation exhibits considerably higher counts of hydrogen bonds. The total number of hydrogen bonds using the CS ensemble is ~3/5 of the number seen using the CL ensemble, which provides support for the argument that chain reorganization is at the root of the main differences between the CS

and CL ensembles in OH-terminated systems. We also note that the results from the CL ensemble for the OH-terminated chains have the same qualitative behavior as the CS ensemble in terms of the change in the total number of inter- and intralayer hydrogen bonds at loads from 0 to 3 GPA. In the CL ensemble the changes in the number of hydrogen bonds are smaller; the smaller decrease in the total number of interlayer hydrogen bonds is also probably due to the ability to reorganize the hydrogen bond network, while the smaller increase in the number of intralayer hydrogen bonds can be attributed to the lower repulsive forces between layers favoring the formation of interlayer hydrogen bonds.

B. Mixed OH-terminated and CH_3-terminated monolayers of variable composition

The frictional properties of monolayers with chains of different surface energy (hydrophobic vs. hydrophilic) depends not only on the composition of the mixture and the nature of the short- or long-ranged interlayer interactions, but also on the *cohesiveness* of the layers and the nature of the short- and long-ranged intralayer interactions.[37] To probe this behavior, we have studied 3 monolayer systems of different surface compositions: $X_{OH} = \{0.25, 0.50, \text{and } 0.75\}$. To simulate the composition $X_{OH} = 0.25$, every other chain in every other row of a pure CH_3-terminated layer was replaced with an OH-terminated chain. For $X_{OH} = 0.75$, every other chain in every other row of a pure OH-terminated layer was replaced by a CH_3-terminated chain. For $X_{OH} = 0.5$, two different surface distributions were studied, the first created by completely replacing every other row of a pure CH_3-terminated surface with a row of OH-terminated chains and the second produced by exchanging every other CH_3-terminated chain in every row with an OH-terminated chain. Since the simulations of pure monolayers showed that the CS and CL ensembles produce essentially the same behavior over a wide range of normal loads, all remaining simulations were performed in the CS ensemble only.

Results for the shear stress as a function of the normal load for all of the mixed monolayers studied are shown in Fig. 7. Similar to the results obtained from AFM experiments of friction in mixed $HS(CH_2)_{15}COOH/HS(CH_2)_{15}CH_3$ monolayers,[37] we find that the profiles for the mixed chains exhibit high friction forces that fall between those of the pure OH- and CH_3-terminated monolayers. In accordance with the behavior seen in the pure monolayers studied in this work, the shear stress profiles for the mixed monolayers show nonlinear behavior at loads up to 1 GPa, after which the profiles exhibit essentially linear behavior with similar coefficients of friction ($\sim$0.1), indicating that other forces play an important role at high pressures. At a constant zero-load (inset of Fig. 7), the shear stress shows a linear dependence with surface composition for $X_{OH} \geq 0.25$, indicating that at low loads the chains remain essentially straight and the interaction between OH-terminated chains dominates the shear stress. At the higher loads of 3 GPa, also reported in the inset of Fig. 7, the data suggest a nonlinear dependence, though we note that the data have non-negligible uncertainties. In order to verify the effect of the hydrogen bonds on the behavior of the shear stress, the average number of hydrogen bonds was calculated, and are reported in Table II and Fig. 8. At zero-load, the data clearly show that the sum of both the intra- and interlayer hydrogen bonds increases linearly with the surface concentration of hydroxyl groups, in agreement with the observed linear dependence of the shear stress on surface concentration at zero-load (inset graph of Fig. 7). The shear stress therefore also has a linear dependency on the sum of the intra- and interlayer hydrogen bonds. Similar behavior was observed experimentally in AFM measurements of $COOH/CH_3$ monolayers with chains of comparable length.[37] We also note Table II confirms that for one of the mixtures at $X_{OH} = 0.50$, there is no possibility to form non-matching hydrogen bonds, because the rows with hydroxyl groups are separated by $\sim$10 Å, and so all hydrogen

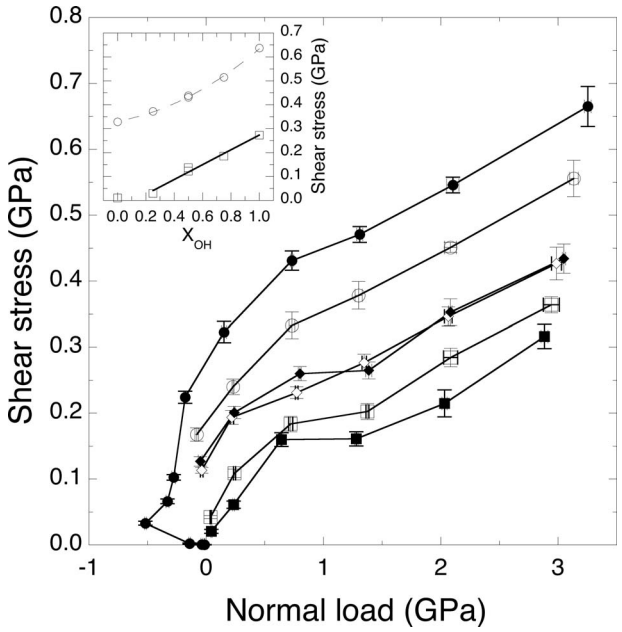

FIG. 7. Shear stress as a function of normal load under sliding at a constant velocity of 10 m/s and 300 K for mixed $-Si(OH)_2(CH_2)_6OH$ and $-Si(OH)_2(CH_2)_5CH_3$ monolayers using the constant separation ensemble. Values for pure $-Si(OH)_2(CH_2)_6OH$ and $-Si(OH)_2(CH_2)_5CH_3$ monolayers are depicted with filled circles and filled squares, respectively. Open circles and open squares represent mixed systems with $X_{OH} = 0.75$ and $X_{OH} = 0.25$, respectively. Filled and open diamonds represent the two distributions of surface chains at $X_{OH} = 0.5$. Lines are provided only as a guide to the eye. (Inset graph) Interpolations of the shear stress at constant load as a function of the surface concentration for OH-terminated chains at normal loads of 3 GPa (circles) and 0 GPa (zero-load) (squares).

TABLE II. Number of hydrogen bonds for mixed monolayers of $-Si(OH)_2(CH_2)_6OH$ and $-Si(OH)_2(CH_2)_5CH_3$ chains at different compositions under sliding at a constant velocity of 10 m/s and 300 K.

	Interlayer		Intralayer	
X_{OH}	Total	Matching	Total	Matching
0.25	11	11	0	0
0.50	51	26	12	0
0.50	66	66	3	3
0.75	94	65	19	4
1.00	147	90	22	8

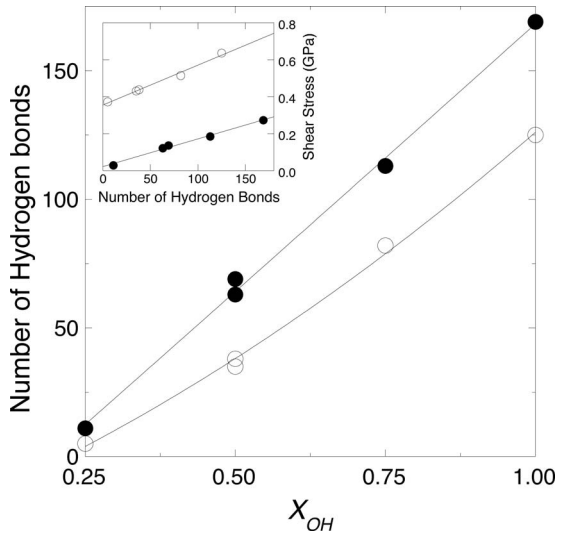

FIG. 8. Sum of intra- and interlayer hydrogen bonds as a function of the surface concentration for mixed $-Si(OH)_2(CH_2)_6OH$ and $-Si(OH)_2(CH_2)_5CH_3$ monolayers sliding at a constant velocity of 10 m/s and 300 K in the constant separation ensemble. Filled and open symbols represent results at 0.15 and 3.25 GPa, respectively. The lines are provided as a guide to the eye and represent linear (0.15 GPa) and quadratic (3.25 GPa) fittings. Inset graph: Shear stresses as a function of the sum of intra- and inter-layer hydrogen bonds. Symbols represent the same states as the main figure.

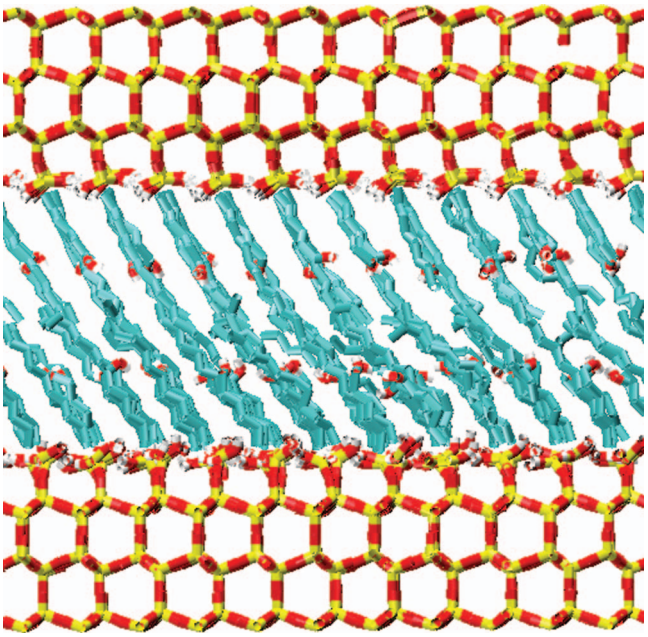

FIG. 9. Snapshot from simulations of mixed $-Si(OH)_2(CH_2)_6OH$ (50%) and $-Si(OH)_2(CH_2)_{11}CH_3$ (50%) monolayers under sliding at constant velocity of 10 m/s and 300 K using the constant separation ensemble at a normal load of 0.15 GPa. Hydrogens linked to the carbon atoms are not shown to facilitate the localization of OH groups. Color scheme is the same as Fig. 1.

bonds (intra- and interlayer) are matching. At higher pressures, the monolayer chains tilt towards the surface and so interactions involving the atoms of the interior CH_2 groups will increase (cf. Fig. 1(d)), the separation between interlayer OH groups decreases, and the interactions due to repulsive van der Waals interactions become more important. This conclusion is supported by both the slight nonlinear behavior observed in the shear stress at 3 GPa shown in the inset of Fig. 7 (less OH and more CH_2 interactions will lower the shear stress) and the similar nonlinear tendency between the monolayer composition and the number of hydrogen bonds, as shown in Fig. 8. Moreover, if the shear stress is plotted as a function of the number of hydrogen bonds (as shown in the inset of Fig. 8), the two weak nonlinearities are counterbalanced, leaving a largely linear relationship between shear stress and number of hydrogen bonds at both 0 GPa and 3 GPa. This shows quite clearly that, at both pressures, there is a component of the shear stress driven by the hydrogen bonding.

C. Mixed OH-terminated and CH_3-terminated chains of variable length

Another way to modify the surface interactions in mixed monolayer systems is to modify the chain length of the CH_3-terminated chains. Depending upon the chain length of the alkyl chains this can create a mobile-bound lubrication system in which the OH-terminated chains provide the bound lubrication layer and the longer alkyl chains provide a mobile component. To investigate this behavior, the sliding behavior and shear stresses of 50:50 mixed OH- and CH_3-terminated chains with $-Si(OH)_2(CH_2)_nCH_3$, where $n = \{5,7,9,11,13,15,$ and $17\}$, were examined and the results presented in Fig. 10.

All the systems studied were found to exhibit lower shear stresses than the pure OH-terminated monolayers, with narrower adhesion zones than those seen in the pure system. Furthermore, as the length of the CH_3-terminated chains is increased, a buffer zone separating the OH-terminated chains of each layer is observed, as seen in Fig. 9 for the mixed system $-(CH_2)_6OH/-(CH_2)_{11}CH_3$. The buffer zone is created by the difference in chain length of the CH_3-terminated chains over the OH-terminated chains. At normal loads near zero, the chains remain parallel to the surface normal indicating that the friction forces are dominated by van der Waals interactions and so the terminal CH_3 groups are primarily participating in the friction interactions. The buffer zone affects noticeably the shear stress at normal loads above ~0.5 GPa. In order to compare the systems directly, in the inset of Fig. 10 we show the shear stress at constant loads of 0 and 3 GPa (extrapolated as needed). At zero loads as the chain length is increased, the shear stress is found to decrease due to conformational ordering; longer chains tend to retain molecular order under sliding, due to higher cohesive forces between the chains.[14,64,65] At a constant load of 3 GPa, a maximum in the shear stress is observed for the system with $-(CH_2)_9CH_3$ chains, after which the shear stress decreases with any further increase in chain length, within the range of chain lengths studied. Given the uncertainties in the original data, as indicated by the error bars in Fig. 10, in order to confirm the observed maximum and explain the differences in the shear stresses as the length of the CH_3-terminated chains is increased at high loads, we have examined how the size of the buffer zone affects the intermolecular interactions between the OH groups. Clearly, as the alkylsilane chain length is increased, a larger buffer zone develops due to the increased

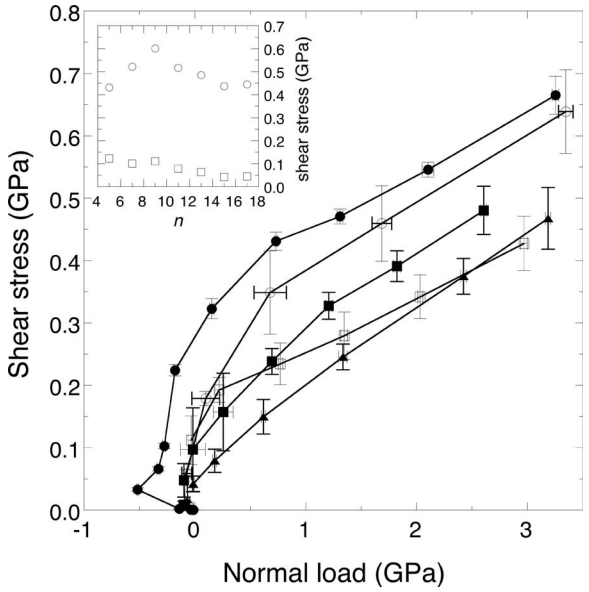

FIG. 10. Shear stress as a function of normal load under sliding at constant velocity of 10 m/s and 300 K for silica coated with mixed $–(CH_2)_6OH$-terminated (50%) and $–(CH_2)_nCH_3$-terminated (50%) chains using the constant separation ensemble. Values for pure $–(CH_2)_6OH$-terminated chains are depicted with filled circles. Open squares represent the mixed systems with $n = 5$, filled squares $n = 7$, open circles $n = 9$, and filled triangles $n = 17$. Lines are provided only as a guide to the eye. (Inset graph) Interpolation of the shear stress at constant normal load as a function of the number of the methylene groups in the $(CH_2)_nCH_3$-terminated chains at normal loads of 3 GPa (circles) and 0 GPa (zero-load) (squares).

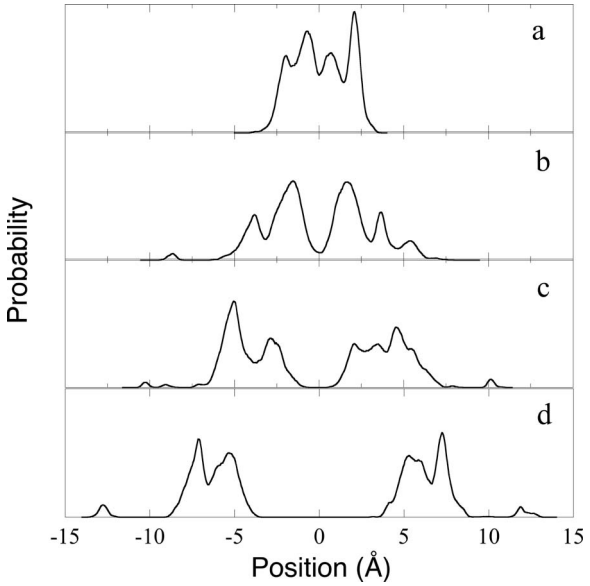

FIG. 11. Distributions of oxygen atoms in $–Si(OH)_2(CH_2)_6OH$ chains along the normal direction for the mixed $–Si(OH)_2(CH_2)_6OH$ (50%) and $–Si(OH)_2(CH_2)_nCH_3$-t (50%) monolayers at 300 K and a constant separation of ~38 Å (normal load ~3 GPa) and a sliding velocity of 10 m/s. (a) $n = 5$, (b) $n = 9$, (c) $n = 11$, and (d) $n = 17$. $z = 0$ indicates the position at the center of the simulated system between the two monolayers.

difference in length between the CH_3-terminated and the OH-terminated chains (whose length is kept constant). The probability of finding oxygen atoms between the monolayers along the normal direction for all systems was examined and the results for $(–(CH_2)_5CH_3)$ (the shortest system studied), $(–(CH_2)_9CH_3)$ (the system showing the maximum shear stress), $(–(CH_2)_{10}CH_3)$ and $(–(CH_2)_{17}CH_3)$ (the longest system studied), are presented in Fig. 11. For the mixed system with $–(CH_2)_5CH_3$ chains, the oxygen atoms are clearly located at the center of the two opposing monolayers ($z = 0$); there is no buffer zone in this system as the OH-terminated chains are slightly longer than the CH_3-terminated chains. As the length of the hydrocarbon chains is increased, the intermolecular separation between the oxygens of each layer increases and the buffer zone develops. For the mixed system with $–(CH_2)_9CH_3$ chains, a small region develops in which the OH groups of opposing monolayers can interact and the separation between the two main peaks is ~3.2 Å. The separation between the nearest peaks increases to ~4.9 Å for the mixed system with $–(CH_2)_{11}CH_3$ chains and to 10.5 Å for the $–(CH_2)_{17}CH_3$ system. The shear stress values in Fig. 10 for the shorter system can therefore be attributed to weak interlayer hydrogen bonds between the oxygen atoms in both monolayers, while the maximum seen for the system with $–(CH_2)_9CH_3$ chains is due to strong interlayer hydrogen bonds as the resulting separation of the OH groups is near optimal for hydrogen bond formation. During sliding, the strong hydrogen bonds in the normal direction are transformed into strong hydrogen bonds in the sliding direction, until the chains move a sufficient distance that the hydrogen bonds break and new hydrogen bonds with the next chain form, producing a pronounced stick and slip behavior as shown from the time profile of the shear stress at ~3 GPa in Fig. 12. For mixed systems of longer chain lengths, the separation between the oxygens in both monolayers is larger than the optimal hydrogen bond distance, and so only weak hydrogen bonds are able to form and the shear stress is therefore lower.

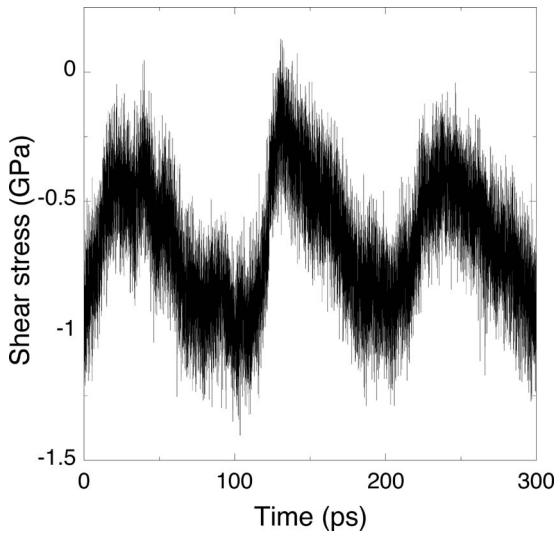

FIG. 12. Shear stress as a function of simulation time for the mixed $–Si(OH)_2(CH_2)_6OH$ (50%) and $–Si(OH)_2(CH_2)_9CH_3$ (50%) monolayer under sliding at a constant velocity of 10 m/s and 300 K using the constant separation ensemble at a normal load ~3 GPa.

IV. CONCLUSIONS

We have performed molecular dynamics simulations to study the frictional behavior of functionalized alkylsilanes coating silica surfaces over a wide range of normal loads at 300 K and a sliding velocity of 10 m/s. Van der Waals and hydrogen bond interactions between the terminal (methyl and hydroxyl) and chain groups (methylene) at high normal loads are found to be the main contributors to the friction forces.

In pure OH terminated surfaces, we find that hydrogen bonds strongly affect the adhesion and sliding behavior. The hydrogen bonds result in wide adhesion zones located between the state of zero-load and the state of zero-load and zero-adhesion. The adhesion zones show low shear stress values due to the fact that the monolayers have long interlayer separations, where only weak Coulombic interactions contribute to the frictional forces. At zero loads, the shear stresses are one order of magnitude higher than the shear stresses seen for CH_3-terminated chains at the same normal load, in agreement with experimental work.[37,38] In the region of positive normal loads, the shear stress increases with the normal load in a nonlinear fashion. When the constant load ensemble is used to study the hydrophilic chains, the shear stress exhibits larger values than those observed in the constant separation ensemble; for OH-terminated monolayers the behavior is opposite to that seen for CH_3-terminated monolayers, as the constant load ensemble allows the chains to reorganize and form stronger hydrogen bond networks, which are more difficult to break and so produce higher friction forces.

The sliding behavior of mixed hydroxyl- and methyl-terminated chains of the same chain length was also studied and showed intermediate behavior between that observed for the pure chains. The shear stress was naturally found to depend on the fraction of the surface that had hydroxyl-terminated chains; close to zero loads, the shear stress increased linearly with the number of hydroxyl-terminated chains, but at high loads, the chains tilt, and interactions with CH_2 groups dominate, which along with repulsive van der Waals interlayer interactions between the hydroxyl groups, produces a slightly nonlinear behavior in the shear stress with increasing hydroxyl-termination.

For mixed monolayers of hydroxyl- and methyl-terminated chains, the chain length of the methyl-terminated chains also affects the behavior of the shear stress at high loads. In simulations performed of mixed $-(CH_2)_6OH$ and methyl-terminated chains of increasing chain length a maximum in the shear stress for the system with $-(CH_2)_9CH_3$ chains was observed. The maximum is seen as the methyl-terminated chains produce a buffer zone of optimal length that facilitates the formation of interlayer hydrogen bonds. At low loads, the methyl-terminated chains do not bend over the shorter OH-terminated chains, keeping the separation distances too large for hydrogen bonds to form.

ACKNOWLEDGMENTS

This work was supported by the Office of Naval Research under Grant Nos. N00014-06-1-0624, N00014-09-1-0334, and N00014-09-10793 and the State of Tennessee. C.M.C. also acknowledges support from the Jacob Wallenberg Foundation and the National Science Foundation through Grant No. OCI-1047828. This research used resources of the National Center for Computational Sciences at Oak Ridge National Laboratory, which is supported by the Office of Science of the Department of Energy under Contract No. DE-AC05-00OR22725, and the National Energy Research Scientific Computing Center, which is supported by the Office of Science of the Department of Energy under Contract No. DE-AC02-05CH11231.

[1] S. H. Kim, D. B. Asay, and M. T. Dugger, Nanotoday **2**(5), 22–29 (2007).
[2] D. Argyris, D. R. Cole, and A. Striolo, Langmuir **25**(14), 8025–8035 (2009).
[3] J. L. Rivera and F. W. Starr, J. Phys. Chem. C **114**(9), 3737–3742 (2010).
[4] D. Argyris, D. R. Cole, and A. Striolo, J. Phys. Chem. C **113**(45), 19591–19600 (2009).
[5] B. Bhushan, J. Vac. Sci. Technol. B **21**(6), 2262–2296 (2003).
[6] W. R. Ashurst, C. Carraro, R. Maboudian, and W. Frey, Sens. Actuators, A **104**(3), 213–221 (2003).
[7] B. Bhushan, Proc. Inst. Mech. Eng., Part J: J. Eng. Tribol. **215**(J1), 1–18 (2001).
[8] R. Maboudian and C. Carraro, Annu. Rev. Phys. Chem. **55**, 35–54 (2004).
[9] B. Bhushan, Philos. Trans. R. Soc. London **366**(1870), 1499–1537 (2008).
[10] J. A. Harrison, G. Gao, J. D. Schall, M. T. Knippenberg, and P. T. Mikulski, Philos. Trans. R. Soc. London **366**(1869), 1469–1495 (2008).
[11] L. C. Zhang and K. Mylvaganam, J. Comput. Theor. Nanosci. **3**(2), 167–188 (2006).
[12] W. R. Ashurst, C. Yau, C. Carraro, R. Maboudian, and M. T. Dugger, J. Microelectromech. Syst. **10**(1), 41–49 (2001).
[13] B. Bhushan, T. Kasai, G. Kulik, L. Barbieri, and P. Hoffmann, Ultramicroscopy **105**(1-4), 176–188 (2005).
[14] B. D. Booth, S. G. Vilt, J. B. Lewis, J. L. Rivera, E. A. Buehler, C. McCabe, and G. K. Jennings, Langmuir **27**(10), 5909–5917 (2011).
[15] B. Booth, S. Vilt, C. McCabe, and G. K. Jennings, Langmuir **25**(17), 9995–10001 (2009).
[16] S. Sambasivan, S. Hsieh, D. A. Fischer, and S. M. Hsu, J. Vac. Sci. Technol. A **24**(4), 1484–1488 (2006).
[17] J. N. Glosli and G. M. McClelland, Phys. Rev. Lett. **70**(13), 1960–1963 (1993).
[18] M. Chandross, G. S. Grest, and M. J. Stevens, Langmuir **18**(22), 8392–8399 (2002).
[19] M. Chandross, E. B. Webb, M. J. Stevens, G. S. Grest, and S. H. Garofalini, Phys. Rev. Lett. **93**(16), 166103 (2004).
[20] C. D. Lorenz, M. Chandross, G. S. Grest, M. J. Stevens, and E. B. Webb, Langmuir **21**(25), 11744–11748 (2005).
[21] P. T. Mikulski, L. A. Herman, and J. A. Harrison, Langmuir **21**(26), 12197–12206 (2005).
[22] C. D. Lorenz, M. Chandross, J. M. D. Lane, and G. S. Grest, Modell. Simul. Mater. Sci. Eng. **18**(3), 034005 (2010).
[23] Y. Liu and I. Szlufarska, Appl. Phys. Lett. **96**(10), 101902 (2010).
[24] K. C. Eapen, S. T. Patton, S. A. Smallwood, B. S. Phillips, and J. S. Zabinski, J. Microelectromech. Syst. **14**(5), 954–960 (2005).
[25] K. C. Eapen, S. T. Patton, and J. S. Zabinski, Tribol. Lett. **12**(1), 35–41 (2002).
[26] E. Hsiao, A. J. Barthel, and S. H. Kim, Tribol. Lett. **44**(2), 287–292 (2011).
[27] E. Hsiao, D. Kim, and S. H. Kim, Langmuir **25**(17), 9814–9823 (2009).
[28] N. Satyanarayana and S. K. Sinha, J. Phys. D **38**(18), 3512–3522 (2005).
[29] N. Satyanarayana, S. K. Sinha, and B. H. Ong, Sens. Actuators, A **128**(1), 98–108 (2006).
[30] S. G. Vilt, Z. Leng, B. D. Booth, C. McCabe, and G. K. Jennings, J. Phys. Chem. C **113**(33), 14972–14977 (2009).
[31] L. Z. Zhang, Y. S. Leng, and S. Y. Jiang, Langmuir **19**(23), 9742–9747 (2003).
[32] Y. H. Liu, X. K. Wang, J. B. Luo, and X. C. Lu, Appl. Surf. Sci. **255**(23), 9430–9438 (2009).
[33] A. Opitz, S. I. U. Ahmed, M. Scherge, and J. A. Schaefer, Tribol. Lett. **20**(3-4), 229–234 (2005).
[34] M. Chandross, C. A. Lorenz, G. S. Grest, M. J. Stevens, and E. B. Webb, JOM **57**(9), 55–61 (2005).

[35]A. Schirmeisen, L. Jansen, H. Holscher, and H. Fuchs, Appl. Phys. Lett. **88**(12), 123108 (2006).
[36]A. Marti, G. Hahner, and N. D. Spencer, Langmuir **11**(12), 4632–4635 (1995).
[37]J. E. Houston and H. I. Kim, Acc. Chem. Res. **35**(7), 547–553 (2002).
[38]N. J. Brewer, B. D. Beake, and G. J. Leggett, Langmuir **17**(6), 1970–1974 (2001).
[39]Y. S. Leng and S. Y. Jiang, J. Am. Chem. Soc. **124**(39), 11764–11770 (2002).
[40]B. Park, M. Chandross, M. J. Stevens, and G. S. Grest, Langmuir **19**(22), 9239–9245 (2003).
[41]W. B. Pearson, P. Villars, and L. D. Calvert, *Pearson's Handbook of Crystallographic Data for Intermetallic Phases* (American Society for Metals, Metals Park, OH, 1985).
[42]R. W. G. Wyckoff, *Crystal Structures* (Wiley, New York, 1963), Vol. 1, pp. 318–319.
[43]K. Kojio, S. R. Ge, A. Takahara, and T. Kajiyama, Langmuir **14**(5), 971–974 (1998).
[44]I. M. Tidswell, B. M. Ocko, P. S. Pershan, S. R. Wasserman, G. M. Whitesides, and J. D. Axe, Phys. Rev. B **41**(2), 1111–1128 (1990).
[45]W. L. Jorgensen, D. S. Maxwell, and J. TiradoRives, J. Am. Chem. Soc. **118**(45), 11225–11236 (1996).
[46]O. A. Mazyar, G. K. Jennings, and C. McCabe, Langmuir **25**(9), 5103–5110 (2009).
[47]A. M. Cione, O. A. Mazyar, B. D. Booth, C. McCabe, and G. K. Jennings, J. Phys. Chem. C **113**(6), 2384–2392 (2009).
[48]C. D. Lorenz, E. B. Webb, M. J. Stevens, M. Chandross, and G. S. Grest, Tribol. Lett. **19**(2), 93–99 (2005).
[49]S. Plimpton, J. Comput. Phys.**117**(1), 1–19 (1995).
[50]P. S. Crozier, R. L. Rowley, and D. Henderson, J. Chem. Phys. **114**(17), 7513–7517 (2001).
[51]W. G. Hoover, Phys. Rev. A **31**(3), 1695–1697 (1985).
[52]S. Nosé, J. Chem. Phys. **81**(1), 511–519 (1984).
[53]S. Nose, Mol. Phys. **52**(2), 255–268 (1984).
[54]M. E. Tuckerman, B. J. Berne, and G. J. Martyna, J. Chem. Phys. **97**, 1990–2001 (1992).
[55]B. Bhushan, *Springer Handbook of Nanotechnology*, 2nd ed. (Springer-Verlag, Heidelberg, 2007).
[56]V. Zaloj, M. Urbakh, and J. Klafter, Phys. Rev. Lett. **82**(24), 4823–4826 (1999).
[57]T. Kreer, K. Binder, and M. H. Muser, Langmuir **19**(18), 7551–7559 (2003).
[58]D. L. Allara, A. N. Parikh, and F. Rondelez, Langmuir **11**(7), 2357–2360 (1995).
[59]A. N. Parikh, D. L. Allara, I. B. Azouz, and F. Rondelez, J. Phys. Chem. **98**(31), 7577–7590 (1994).
[60]M. S. Kelkar, J. L. Rafferty, E. J. Maginn, and J. I. Siepmann, Fluid Phase Equilib. **260**(2), 218–231 (2007).
[61]A. K. Soper, Chem. Phys. **258**(2-3), 121–137 (2000).
[62]See supplementary material at http://dx.doi.org/10.1063/1.4729312 for animations.
[63]B. Bhushan, *Modern Tribology Handbook* (CRC, Boca Raton, FL, 2001).
[64]A. Lio, D. H. Charych, and M. Salmeron, J. Phys. Chem. B **101**(19), 3800–3805 (1997).
[65]M. T. McDermott, J. B. D. Green, and M. D. Porter, Langmuir **13**(9), 2504–2510 (1997).